eCHORD orientation mapping of bio-inspired alumina down to 1 kV

Clément Lafond, T. Douillard, Hassan Saad, Sylvain Deville, Sylvain Meille, Ph Steyer, Sophie Cazottes, Cyril Langlois

eCHORD orientation mapping of bio-inspired alumina down to 1 kV

C. Lafond[1], T. Douillard[1], H. Saad[2], S. Deville[2,3], S. Meille[1], Ph. Steyer[1], S. Cazottes[1], C. Langlois[1*]

[1]Univ Lyon, INSA Lyon, UCBL, CNRS, MATEIS, UMR5510, 69621 Villeurbanne, France

[2]Laboratoire de Synthèse & Fonctionnalisation des Céramiques, UMR3080 CNRS-Saint-Gobain CREE, Saint-Gobain Research Provence, Cavaillon 84306, France

[3]Univ Lyon, Université Claude Bernard Lyon 1, CNRS, Institut Lumière Matière, 69622 Villeurbanne, France

***corresponding author**

Abstract:

Orientation mapping using Electron Back Scattered Diffraction (EBSD) is limited in its spatial resolution by the acceleration voltage, usually higher than 5 kV. In the present work, we present for the first time an orientation mapping at 1 kV obtained by the eCHORD approach (**e**lectron **CH**anneling **OR**ientation **D**etermination) on a lamellar bio-inspired alumina sample. Texture results extracted from the 1 kV eCHORD mapping are in very good agreement with texture measurements obtained by EBSD at 15 kV on the same sample. Potential issues associated to such a low accelerating voltage for eCHORD measurements are discussed.

Keywords: orientation imaging microscopy (OIM) ; eCHORD ; electron backscattering diffraction (EBSD) ; ceramics ; metal and alloys.

Manuscript:

1. Introduction

Mapping the grain orientations of polycrystalline materials brings crucial information when studying the relationships between microstructure and properties. Among different orientation mapping approaches able to detect individual grains, from optical [1] to diffraction [2,3] and ion channeling [4], the use of Electron Back Scattered Diffraction (EBSD) in a Scanning Electron Microscope (SEM) has been a milestone in the development of crystallographic characterizations for studying, for instance, recrystallization or phase transitions. Taking advantage of the growing capabilities of modern computers, the technique is now fully automated and widely used. Nevertheless, even if EBSD is well established in the materials science and geology communities, efforts are still needed to improve the technique toward a better spatial resolution. The underlying idea is to enable the characterization of ultrafine microstructures like heavily deformed materials or ultrafine grain size distribution, without turning to Transmission Electron Microscopy (TEM) or Transmission Kikuchi Diffraction (TKD) which require complex sample preparation. Concerning EBSD, one strategy is to decrease the accelerating

voltage in order to reduce the interaction volume under the probed surface, increasing the spatial resolution. However, the Kikuchi pattern quality decreases rapidly and the standard indexation routine fails to recover the grain orientations [5]. The actual limit found in the literature is 5 kV for a standard configuration, and 3 kV using a specific detector [6]. At these acceleration voltages, a special dictionary indexing approach must be used to index the grains [5,7].

The "electron CHanneling ORientation Determination" (eCHORD) approach [8,9] is not subjected to such limitations at low voltage. It relies on the acquisition of an image series using back scattered electrons (BSE), and it has been shown that the channeling contrast was still present at low voltages in BSE images [10]. In the current paper, we show that orientation mapping at voltages as low as 1 kV is possible on a highly textured alumina specimen. On this material, EBSD measurements were also carried out at higher voltage. Texture information extracted from different areas of a polished surface were determined by EBSD and eCHORD for comparison purpose. The present work hence constitutes the first orientation mapping obtained at an acceleration voltage of 1 kV.

2. Materials and Methods

2.1 Bio-inspired alumina

All the experiments have been carried out on a bio-inspired nacre-like alumina with a lamellar structure as initially described in Bouville *et al*. [11]. This material is made of 95vol% of aligned alumina platelets (trigonal structure, space group 167), with an interphase made of a glassy phase and alumina nanoparticles. A simplification of the processing of such materials has been recently made, without platelets pre-alignment step [12]. Uniaxial pressing during field assisted sintering has been shown to ensure an efficient platelet alignment, even if some local disorientations and some broken platelets can be noted in the final microstructure. A fine quantification of the quality of platelets alignment as well as their size distribution is necessary to properly characterize the material in order to optimize the process.

2.2 eCHORD acquisition

The eCHORD BSE image series has been obtained using the protocol described in Lafond *et al.* [8]. The microscope was a ZEISS NVision 40 SEM (Carl Zeiss Microscopy GmbH, Oberkochen, Germany). It is worth noting that the Variable Pressure mode was deliberately not used for the eCHORD image acquisition. The EsB detector (Energy and angle Selective BSE detection) inside the electron column was used to detect the BSE signal within an energy range from 0.8 kV to 1 kV thanks to a built-in grid that can be polarized from 0 to 1500 V. Concerning the image series acquisition, a rotation from 0° to 360° was performed with a sample tilt of 15° and a rotation step of 2°. For each image, the pixel size was 56 nm and a time-per-frame of 10.2 seconds was used. The eCHORD image series was post-treated

as described in Lafond *et al*. [8], according to the following steps : 1/ image series alignment, 2/ denoising, 3/ background removal. For indexing the raw data, a theoretical database of 60 million profiles was computed with an accelerating voltage of 1 kV, using the EMsoft program suite [5]. EBSD measurements were possible on the same sample, for comparison sake, but not on the eCHORD region of interest (ROI) due to contamination issues, i.e. deposition of carbonaceous material over the sample surface scanned by the electron beam. EBSD mapping was performed using Nordlys F detector from Oxford Instruments with an accelerating voltage of 15 kV and a step of 80 nm while the acquisition speed was 150Hz.

3. Results

3.1 Expected spatial resolution from Monte-Carlo simulations

It is first necessary to evaluate the benefits expected from a lower accelerating voltage in terms of spatial resolution for nacre-like alumina. Monte-Carlo simulations were carried out, comparing the escape depth and the surface exit diameter of the detected BSE for 5 kV and 1 kV, with an incidence angle of 15° and Al_2O_3 sapphire data (atomic numbers and density). Two widely used programs were operated for these simulations: CASINO [13] and HURRICANE (from SAMx® http://www.samx.com/index.html.en), the two programs providing complementary information. The results presented in figure 1.a and 1.b were obtained with CASINO and show the distributions describing the maximum depth reached by the primary electrons before being backscattered and detected, for 5 kV and 1 kV respectively. This BSE maximum escape depth drops from 100nm to 10 nm when going down to 1 kV. The results presented in figure 1.c and 1.d were obtained with HURRICANE and show that, reducing the acceleration voltage from 5 kV to 1 kV, the BSE emergence area on the specimen surface shrinks from a radius around 300 nm to 30 nm when considering the total BSE signal. Moreover, at 1 kV, when filtering and detecting BSE over 800 V, this radius drops to 20 nm. It means that, for each eCHORD image series at such a low voltage and with energy filtering, very fine details could be kept in each image, provided a sufficiently small pixel size. More generally, the advantages of energy filtering on spatial resolution are discussed in Brodusch *et al.*[14].

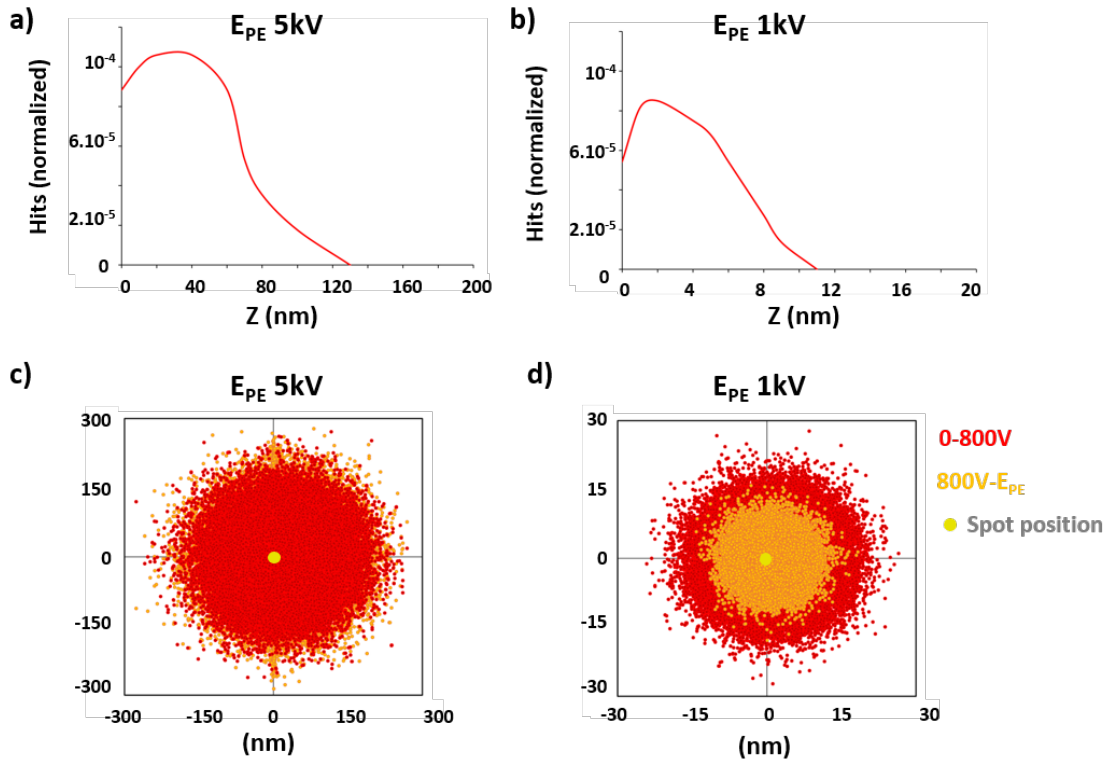

Figure 1: *(a) and (b) BSE escape depth (Z) distribution computed from Monte-Carlo simulations (CASINO v2.51 ; 5.10^5 electron trajectories in alumina ; beam tilt of 15°) at (a) primary electron energy E_{PE} of 5 kV and (b) primary electron energy E_{PE} of 1 kV. (c) and (d) Monte Carlo simulations with HURRICANE program (same conditions as CASINO simulations) evidencing BSE emergence area on the specimen surface with a focus on the effect of a 800 V – 1 kV high-pass energy filtering: red spots correspond to BSE with an energy ranging from 0V to 800 V ; orange spots correspond to BSE with an energy ranging from 800V to 1 kV.*

3.2 eCHORD orientation mapping and texture analysis

The first image of the eCHORD image series is presented in Figure 2.a. The channeling contrast is clearly visible in the image even at such a low accelerating voltage. It is first crucial to verify if the agreement between the experimental profiles and the dynamic simulation at such low voltage is similar to what is obtained at higher voltages [8], and eventually filter the measurements to discard misindexations. For eCHORD, the metric used to compare experimental and theoretical intensity profiles during the indexation operation is a distance defined as [4,8]:

$$d = 1 - DotProduct(experimental\ profile\ ;\ best\ fit\ theoretical\ profile)$$

It can be used to roughly evaluate the indexation quality, in absence of a more accurate quality factor (under development). From previous studies with a comparison with EBSD [8], a distance value below 0.05 was accepted as a valid indexation. Consequently, the distance map computed in each pixel of

the region of interest (ROI) has been thresholded with this value to detect misindexations. The thresholded distance map is shown in Figure 2.b. with misindexed positions (according to the distance criterion) represented in white. Misindexed positions correspond quite logically to grain boundaries, but also sometimes to whole grains. The distribution of distance values in the map is represented in Figure 2.c to evaluate the proportion of misindexed measurements. To shed light on the actual signification of this distance criterion, the comparison of two profiles at two different distances are represented on Figure 2.d. The one on top with a distance slightly above the distance limit shows some misalignments between intensity peaks. On the contrary, for the comparison shown on the plot at the bottom with a distance corresponding to the peak value of the distribution at d = 0.032, the intensity peaks are well aligned which confirm that the indexation procedure was successful.

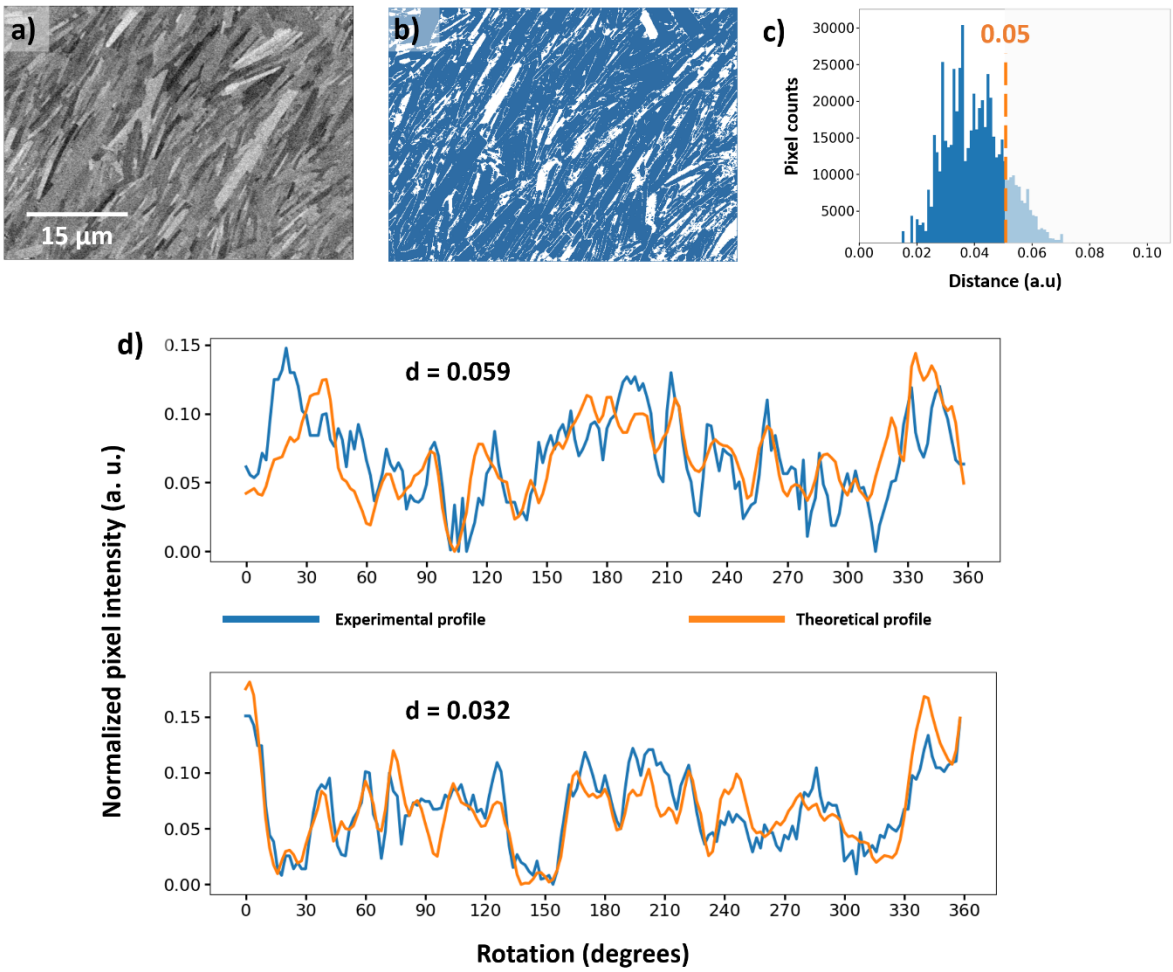

***Figure 2**: eCHORD raw results obtained at 1 kV. a) first image of the BSE image series. b) Distance map of the region of interest (ROI) with a thresholding at d = 0.05 (see text for a definition of "distance"). Positions in white correspond to distances above 0.05 (arbitrarily considered as misindexed) whereas positions in blue correspond to distances below 0.05 (considered as correctly indexed). c) Distribution of distances in the ROI with an orange vertical visual marker at d = 0.05. d) Two examples of indexation between experimental intensity profile (in blue) and indexed theoretical intensity profile (in orange). The top plot is an example of arbitrarily discarded orientation indexation due to a distance d = 0.059*

above the aforementioned limit. The bottom plot demonstrates a typical agreement between experimental and theoretical profiles with a distance d = 0.032, which is the peak value of the distribution in c).

As a consequence, all measurements with a distance *d* between theoretical and experimental profiles higher than 0.05 have been discarded from the following data treatments. Then, considering the average grain size in the specimen, all grains with an apparent area containing less than 30 pixels (~0.1 µm²) have been discarded too. From this filtered input data, the pole figures (PF) for planes (0001), (10-10) and (10-12) in the trigonal system of sapphire alumina have been computed to analyse the orientations of the platelets in the specimen (see Figure 3.a). The PFs show a strong texture: the **c** axis of the crystals is mainly oriented along the direction **n** normal to the platelets, indicated on Figure 3.a and 3.b, which corresponds to the pressing of the sample during its fabrication [12]. This texture direction has been used as a reference direction for the Inverse Pole Figure (IPF) in Figure 3.b. The color code of the IPF shown in Figure 3.a (bottom right) allows identifying the platelets that are not aligned with the direction **n**.

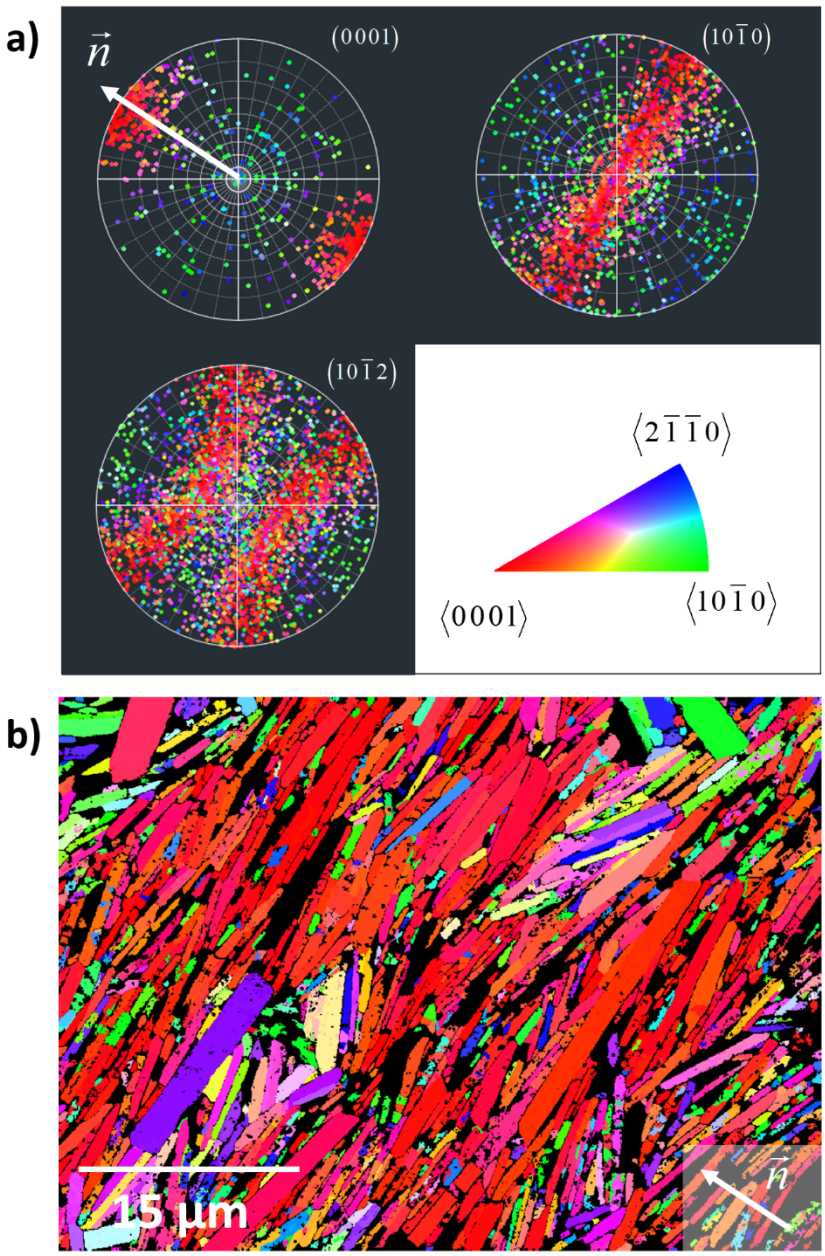

Figure 3: *Orientation analysis. a) Pole figures for crystal planes (0001), (10-10) and (10-12), evidencing a strong texture in the region of interest with the* ***c*** *crystal axis along the represented direction* ***n*** *(white arrow). b) Inverse pole figure (IPF) map, using as a reference the direction* ***n*** *indicated on a) by a white arrow. The superimposed direction* ***n*** *corresponds to the average direction orthogonal to the* Al_2O_3 *platelets. On this IPF, black color corresponds to filtered data not considered for the texture analysis. Color coding of the IPF map is presented on the bottom right of a).*

3.3 EBSD results

EBSD mapping at 1 kV is currently not feasible. Therefore, a direct comparison between the two techniques cannot be performed on the same interaction volumes. In order to validate in a statistical way the orientations found using eCHORD, the texture data obtained using the two mapping

technique were compared. Figure 4 presents the texture analysis obtained from an EBSD mapping at 15 kV. The same analysis as for the eCHORD measurements has been carried out, with the same conclusion about a strong texture in this material, with the **c** axis of the hexagonal lattice perpendicular to the platelets composing the microstructure.

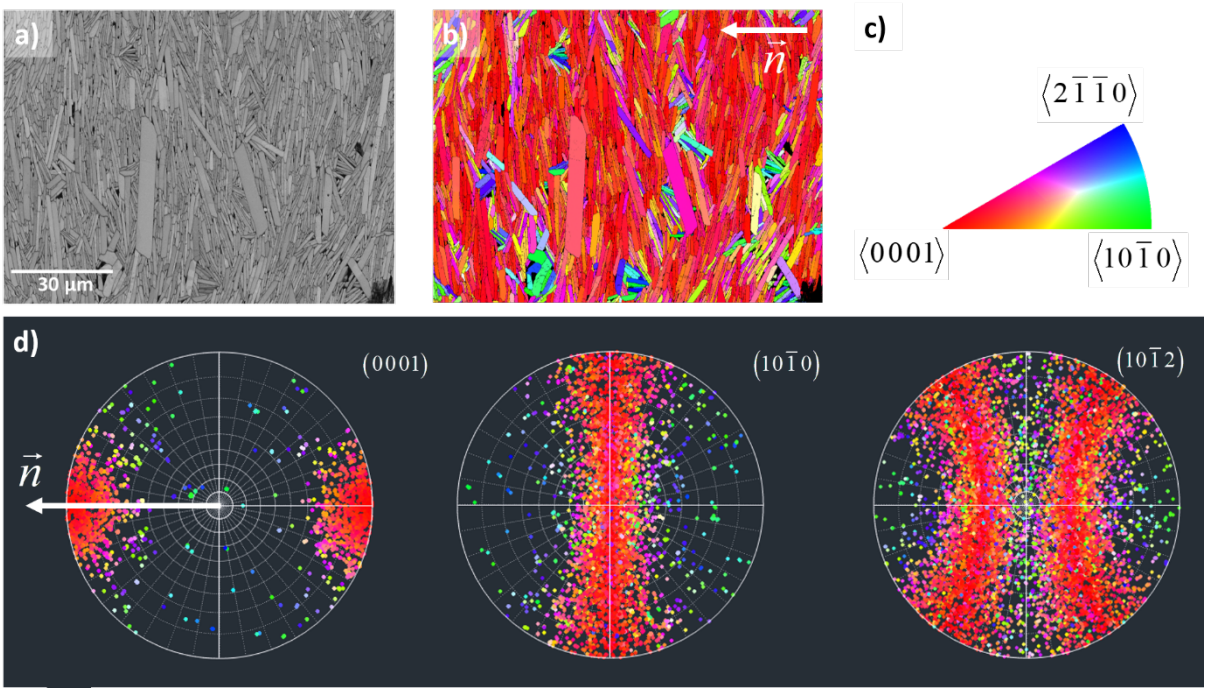

Figure 4: *EBSD mapping results at 15 kV. a) Kikuchi band contrast image. b) Inverse pole figure (IPF) map, using as a reference the direction **X**, horizontal on the image and normal to the platelets. c) Color coding of the IPF map presented on b). d) Pole figures for crystal planes (0001), (10-10) and (10-12), evidencing a strong texture in the region of interest.*

4. Discussion

4.1 Toward orientation mapping at high spatial resolution

Results from eCHORD and EBSD methods are in good agreement concerning the local texture determination on the alumina sample. It means that, for most of the platelets, the crystallographic orientation has been correctly determined by eCHORD even for such low accelerating voltage. One can conclude that the dynamical diffraction simulations were accurate enough to enable the mapping at 1 kV. This result is a step towards high spatial resolution orientation mapping in the SEM using eCHORD because 1/ the core of the eCHORD approach, which is the experimental occurrence of the channeling effect as well as its correct simulation, is validated for low accelerating voltage on this material, and 2/ the Monte-Carlo simulations predict a spatial resolution about twenty nanometers. Of course, both aspects must be evaluated when considering the use of eCHORD to characterize other materials, especially fine microstructures typical from highly deformed [15] ot nano-twinned [16] materials, or thin film with a thickness of few tens of nanometers[17]. Finally, it is worth noting that orientation

maps with an improved spatial resolution could be of great help when carrying out Electron Channeling Contrast Imaging for studying crystalline defects and deformation mechanisms[18,19].

To take full advantage of the improved spatial resolution at low voltage, it is necessary to adapt the pixel size in the image series to the BSE emergence area. The image pixel size is a function of both SEM magnification and image sampling. Actually, it is not too problematic as, for a 1000x1000 pixels image, a polaroid magnification of 10 kX is nearly enough to reach a pixel size of 10nm. However, this ultimate spatial resolution is slightly degraded due to the image post-treatments, particularly the registration of the image series, but can still confer a spatial resolution of few tens of nanometers in a routine way.

4.2 Challenges and application limitations

Although the agreement between experimental and theoretical intensity profiles was good enough to allow for mapping the orientations for the alumina sample, the correspondence is not as remarkable as for accelerating voltages in the range 10 - 15 kV on aluminum [8,9]. Actually, stronger beam-specimen interactions occur at low accelerating voltage, which increase dynamical effects in the diffracted intensities. This highlights the need for refinements of Monte-Carlo simulations to correctly describe beam-specimen interactions at low accelerating voltage [20–22] as well as an improved description of the energy spectrum of the BSE signal to get more accurate ECP simulation [23,24]. Moreover, such dynamical effects are even more pronounced for higher atomic numbers (Z). These simulation aspects could constitute a challenge when dealing with heavy crystallographic phases.

Imaging a surface with a low energy electron beam results usually in a poor signal-to-noise ratio, which has been degraded further by energy filtering in this study. Hopefully, two BSE detector structures have recently demonstrated promising results with high efficiency for low accelerating voltages: scintillator-photomultiplier [16] and solid-state photodiode detector technology [17–19]. For both of them, there are recent reports of high-resolution detection down to 1 kV and below. Deceleration of probe beam by stage bias potential, which is another way to produce low voltage imaging, has also to be explored [20]. Combined with the eCHORD procedure, these new developments may ease orientation mapping at low acceleration voltages in the future. It is also worth mentioning that, because eCHORD relies on electron diffraction, the signal is strongly dependent on the scattering power of the sample, which increases with the atomic number of the elements composing the specimen. From the point-of-view of signal-to-noise ratio, orientation mapping with eCHORD should then be facilitated for specimen with high atomic number.

An additional drawback to low beam energy operation consists in the sensitivity to so-called contamination effects [25]. If such a contamination layer grows on the surface during the acquisition, it may mask the channeling contrast of the specimen because the crystalline proportion in the reduced

interaction volume will decrease. If polishing residues are present on the surface, the channeling signal may vanish for the same reason. Special care must then be implemented for sample preparation, and the use of RF plasma cleaning has to be considered as well as broad ion beam polishing to reduce both effects.

It is also necessary to consider several phenomena associated with accelerating voltages under 1 kV, among which the yield of the BSE signal as a function of the accelerating voltage and the atomic number. Z-contrast reversal has been reported for instance [26], or yield peaks at specific voltages that could be used to fine tune the experimental parameters to take advantage from it [27].

4.3 Application to other materials classes

Some guidelines emerge from the aforementioned limitations concerning low-voltage eCHORD experiments. For any crystalline materials (metals, ceramics, geological materials), the sample preparation must be carried out with special care, with a criterion being the observation of the channeling contrast in the BSE images. Then, the atomic number drives two important aspects: for increasing atomic numbers, the signal-to-noise ratio increases too and the spatial resolution is improved. Finally, working at low accelerating voltage limits charging artefacts which is advised for non-conductive samples like ceramics or geological materials. It enhances also the spatial resolution at the expense of the signal-to-noise ratio. As a consequence, the accelerating voltage should the highest possible with a limit fixed by charging artefacts and the size of the microstructural features to be mapped.

5. Conclusion

To sum up this work, for the first time an orientation mapping at an accelerating voltage of 1 kV has been carried out on an alumina sample in a SEM. The validity of the measurements relies on a careful examination of the agreement between experimental BSE signature and simulated ones as well as a texture calculation comparison with EBSD on the same sample. This successful experiment paves the way for improving the spatial resolution of orientation mapping on all classes of crystalline materials by the use of a drastically reduced acceleration voltage and energy filtering at the signal detection level. Due to the reduced interaction volume, it will become possible to characterize nanometric structural features for light materials without turning to TKD or TEM. It is especially true for light metals like aluminum or magnesium [28]. Orientation mapping of deposited films with a very low thickness will also be facilitated using low voltage eCHORD due to a reduced interaction depth. Mapping results on fine-grained and deformed microstructures should also be improved for the same reason. Concerning insulating materials, the possibility to map the orientations at low voltage with eCHORD will certainly ease the microstructure characterizations on these materials because the artefacts due to charge accumulation at the surface are strongly reduced at 1 kV.

Declaration of Competing Interest

The authors declare no conflict of interest. S Deville is an editor for Materialia but was involved in neither the handling nor the evaluation of the manuscript.

Acknowledgment

Thanks are due to the CLYM (www.clym.fr) for access to the ZEISS NVision 40 scanning electron microscope. C. Lafond thanks the French Ministry of Higher Education and Research for his PhD grant. We are also grateful for the financial support from the Agence Nationale pour la Recherche (ANR-16-CE08-0006 BICUIT, program DS0303-2016).

References

[1] B. Gaskey, L. Hendl, W. Xiaogang, M. Seita, Acta Mater. 194 (2020) 558–564.
[2] W. Ludwig, A. King, M. Herbig, P. Reischig, J. Marrow, L. Babout, E.M. Lauridsen, H. Proudhon, J.Y. Buffière, JOM 62 (2010) 22–28.
[3] E.F. Rauch, M. Veron, Mater. Werkst. 36 (2005) 552–556.
[4] C. Langlois, T. Douillard, H. Yuan, N.P. Blanchard, A. Descamps-Mandine, B. Van de Moortèle, C. Rigotti, T. Epicier, Ultramicroscopy 157 (2015) 65–72.
[5] S. Singh, M. De Graef, Microsc. Microanal. 23 (2017) 1–10.
[6] F. Wang, M.P. Echlin, A.A. Taylor, J. Shin, B. Bammes, B.D.A. Levin, M. De Graef, T.M. Pollock, D.S. Gianola, Ultramicroscopy 220 (2021) 113160.
[7] M. De Graef, IOP Conf. Ser. Mater. Sci. Eng. 891 (2020) 012009.
[8] C. Lafond, T. Douillard, S. Cazottes, P. Steyer, C. Langlois, Ultramicroscopy 186 (2018) 146–149.
[9] C. Lafond, T. Douillard, S. Cazottes, M. De Graef, P. Steyer, C. Langlois, Ultramicroscopy 208 (2020) 112854.
[10] Š. Mikmeková, K. Yamada, H. Noro, Microscopy 62 (2013) 589–596.
[11] F. Bouville, E. Maire, S. Meille, B. Van de Moortèle, A.J. Stevenson, S. Deville, Nat. Mater. 13 (2014) 508–514.
[12] H. Saad, K. Radi, T. Douillard, D. Jauffres, C.L. Martin, S. Meille, S. Deville, Materialia 12 (2020) 100807.
[13] D. Drouin, A.R. Couture, D. Joly, X. Tastet, V. Aimez, R. Gauvin, Scanning J. Scanning Microsc. 29 (2007) 92–101.
[14] N. Brodusch, H. Demers, R. Gauvin, Field Emission Scanning Electron Microscopy: New Perspectives for Materials Characterization, Springer, 2017.
[15] A. Bachmaier, R. Pippan, O. Renk, Adv. Eng. Mater. 22 (2020) 2000879.
[16] L. Sun, X. He, J. Lu, Npj Comput. Mater. 4 (2018) 6.
[17] P. Rasmussen, R. Berlia, R. Sarkar, J. Rajagopalan, Materialia 15 (2021) 100994.
[18] F.D. Luca, H. Zhang, K. Mingard, M. Stewart, B.M. Jablon, C. Trager-Cowan, M.G. Gee, Materialia 12 (2020) 100713.
[19] G. L'hôte, C. Lafond, P. Steyer, S. Deschanel, T. Douillard, C. Langlois, S. Cazottes, Scr. Mater. 162 (2019) 103–107.
[20] A.M.D. Assa'd, M.M. El Gomati, Scanning Microsc. 12 (1998) 185–192.
[21] M.M. El Gomati, C.G.H. Walker, A.M.D. Assa'd, M. Zadražil, Scanning 30 (2008) 2–15.
[22] J. Pierron, C. Inguimbert, M. Belhaj, T. Gineste, J. Puech, M. Raine, J. Appl. Phys. 121 (2017) 215107.
[23] F. Ram, M. De Graef, Phys. Rev. B 97 (2018) 134104.
[24] A. Winkelmann, T.B. Britton, G. Nolze, Phys. Rev. B 99 (2019) 064115.
[25] A. Vladar, M. Postek, Microsc. Microanal. 11 (2005) 764–765.

[26] R. Böngeler, U. Golla, M. Kässens, L. Reimer, B. Schindler, R. Senkel, M. Spranck, Scanning 15 (1993) 1–18.
[27] J. Rattenberger, J. Wagner, H. Schröttner, in: Instrum. Methodol., Facultas, 2009, pp. 167–168.
[28] A. Tripathi, S. Zaefferer, Ultramicroscopy 207 (2019) 112828.